EPJ Appl. Metamat. **7**, 8 (2020)

https://doi.org/10.1051/epjam/2020008

EPJ Applied Metamaterials

Available online at:
epjam.edp-open.org

RESEARCH ARTICLE

OPEN ACCESS

X-band metamaterial absorbers based on reduced graphene oxide-silicon carbide-linear low density polyethylene composite

Pankaj Bora[1], Utpal Jyoti Mahanta[2], Jayanta Kumar Sarmah[3], and Jyoti Prasad Gogoi[1,*]

[1] Department of Physics, Kaziranga University, Jorhat 785006, India
[2] Department of Physics, Sibsagar College, Sivasagar 785665, India
[3] Department of Chemistry, Kaziranga University, Jorhat 785006, India

Received: 13 October 2020 / Accepted: 30 November 2020

Abstract. Graphene oxide obtained by Hummer's method is used to synthesize reduced graphene oxide (RGO) using chemical and thermal treatment method. Flexible composites of RGO-Silicon carbide (SiC)-Low density polyethylene (LLDPE) in different wt.% ratios of fillers are characterized for complex permittivity and permeability in X-band. A metamaterial design of ring shaped with four stripe structure is designed on developed substrate as well as standard FR4 substrate and simulated using EM simulator, CST Microwave Studio. Simulated results showed shifting of resonant peak frequency from C-band frequency for FR4 substrate to X-band for developed substrates signifying a role of microwave constitutive properties of the dielectric spacer. The fabricated metamaterial structure on RGO-SiC-LLDPE composite of thickness 0.7 mm shows a $S_{11} \sim -25$ dB at 10.7 GHz with maximum absorption of 96.7%. Thus, the developed meta-material design showing a potential application in microwave applications.

Keywords: Reduced graphene oxide / silicon carbide / meta material / microwave absorber

1 Introduction

Simultaneous operation of microwave components in high frequencies wireless communication system experienced electromagnetic interference (EMI) and demands microwave absorber to ascertain electromagnetic compatibility issues [1]. Conventional conductor backed microwave absorbers (MA) depends on its electromagnetic constitutive parameters viz. complex permittivity $\varepsilon_r(\omega)$ and permeability $\mu_r(\omega)$, and thickness (d) and the performance efficiency is estimated by reflection loss (RL_c) using transmission line model [2] and expressed as $RL_c = 20\log\left|\frac{Z_{in}(\omega)-377}{Z_{in}(\omega)+377}\right|$ where $Z_{in}(\omega) = \eta_i \frac{Z_{i-1}+\eta_i \tanh \gamma_i d_i}{\eta_i + Z_{i-1}\tanh\gamma_i d_i}$ is the input impedance. The challenges in conventional MA are adequate absorption ~ -10 dB within limited thickness and specific absorption properties of selective absorbing material fulfilling impedance matching to free space [3]. Meta-material absorber (MMA) due to their exotic electromagnetic properties derived from its unit cell geometric configuration finds wide applications in millimeter [4], the microwave [5,6], and the THz [7] regimes. Conventional MMA are composed of a tri-layer system consist of a metallic top layer periodically patterned in various shape viz. ring, cross, patch etc., a continuous metallic plates bottom layer and a dielectric spacer between them and the absorption mechanism is the coupling between the incident EM field and EM field induced by resonators as demonstrated by Landy et al. [5]. Meta-material structure described as effective medium parameters $\varepsilon_{r(eff)}(\omega)$ and $\mu_{r(eff)}(\omega)$ facilating surface impedance matching to free space as $Z(\omega) = \sqrt{\frac{\mu_{r(eff)}\mu_0}{\varepsilon_{r(eff)}\varepsilon_0}}$ and its reflectivity $|S_{11}(\omega)| = \left|\frac{Z(\omega)-Z_0}{Z(\omega)+Z_0}\right| \to 0$ and thereby increasing the absorptivity $A(\omega)$ as indicated by the relation $A(\omega) = 1 - |S_{11}(\omega)|^2 - |S_{21}(\omega)|^2 = 1 - |S_{11}(\omega)|^2$, since transmission is not allowed by back metallic plane. Further, the dielectric spacer contribute the dielectric loss to dissipate the EM wave energy absorbed [5] and increasing the dielectric thickness (d) increase the absorption bandwidth (B) expressed [8] as $B \cong \frac{4R_0}{\omega d|\mu_r - \varepsilon_r|}$ where R_0 is the lowest possible reflectivity. Extensive work has been performed on development of multiband and broadband MMA with changing MM's design, employing ultrathin resistive spacer sheets and MM design [9–17]. Mostly, the reported research on MMA are rigid dielectric substrates like FR4, silicon wafers and rigid metallic (Cu) back layers [18–27] and emphasize on meta material unit cell design with limited study on the role of dielectric spacer properties on microwave absorption. A flexible meta-material

* e-mail: jpgogoi2013@gmail.com

absorber consisting of linear low density polyethylene (LLDPE) substrate with circular rings unit cell made up of expanded graphite flakes was reported to show 98.9% absorption at 11.22 GHz with FWHM of 2.49% along with a reflection loss of −24.51 dB at 11.56 GHz with −10 dB bandwidth of 0.39 GHz (3.37%) [28]. Incorporation of filler materials in the dielectric composite may influence the propagation of incident microwave and give an overall effect of the metamaterial structure. The potential microwave absorbing fillers materials could be reduced graphene oxide (RGO) [29] and Silicon carbide (SiC) [30] which shows efficient absorption along with good physical properties. In the present study, a novel metamaterial unit cell is design and developed on a novel flexible dielectric substrate consisting of reduced graphene oxide (RGO)-Silicon carbide (SiC)-linear low density polyethylene (LLDPE) with a view to enhance dielectric loss and reduce thickness. Composites material consisting of RGO and SiC in different weight ratios (10, 20 and 30 wt.%) with LLDPE matrix were prepared and characterize in the frequency range 8.2–12.4 GHz. A ring shape with four stripe structure was designed over the developed composites and simulated in the X-band. Optimized design structure was fabricated and tested for microwave absorption in the X-band. To study the role of substrate the similar metamaterial unit cell is design on standard FR4 substrate and compare the microwave absorption results in the X-band.

2 Experimental

2.1 Synthesis of graphene oxide/reduced graphene oxide

Initially, graphene oxide (GO) was synthesized by Hummers method through oxidation of graphite [31,32]. The stepwise preparation is given as follows: Graphite powder (2 g) and $NaNO_3$ (2 g) were mixed in 50 mL of H_2SO_4 (98%) in a 1000 mL volumetric flask kept under at ice bath (0–5 °C) with continuous stirring. The mixture was stirred for 2 h at this temperature and potassium permanganate (6 g) was added to the suspension very slowly. The rate of addition was carefully controlled to keep the reaction temperature lower than 15 °C. The ice bath was then removed, and the mixture was stirred at 35 °C until it became pasty brownish and kept under stirring for 2 days. It is then diluted with slow addition of 100 ml water. The reaction temperature was rapidly increased to 98 °C with effervescence, and colour changed to brown. Further this solution was diluted by adding additional 200 ml of water stirred continuously. The solution is finally treated with 10 mL H_2O_2 to terminate the reaction by appearance of yellow colour. For purification, the mixture was washed by rinsing and centrifugation with 10% HCl and then deionized (DI) water several times. After filtration and drying under vacuum at room temperature, the graphene oxide (GO) was obtained as a powder. The developed (GO) is further dispersed in 400 mL water under ultrasonic treatment till a homogeneous brown GO aqueous suspension was obtained [32]. The pH level of the suspension is maintained at 10 using $NH_3.H_2O$ and hydrazine hydrate was added in the ratio of 10:7 to GO and heated at 80°C for 24 h to produce a black colour predicted which was washed with methanol and water and dried at 80 °C for 24 h. The final product obtained is RGO.

Table 1. RGO-SiC-LLDPE composites sample code.

Samples/wt.%	LLDPE	SiC	RGO
Sample A	90	5	5
Sample B	80	10	10
Sample C	70	20	10

2.2 Development of flexible RGO-SiC-LLDPE substrate

Synthesized RGO was mechanically mixed with powder SiC (supplied by Akshar Chem) and Linear low-density polyethylene (LLDPE) in different weight ratios (5-5-90 wt.%, 10-10-80 wt.% and 10-20-70 wt.%), and poured separately in a cavity for heat treatment at 100°C using hydraulic press with pressure ∼1.5 tons. Pellets of dimensions, 10.16 mm × 22.86 mm × 2 mm for microwave characterization in the X-band. LLDPE due to its flexibility, good tensile strength and low water absorbance was considered as base matrix of the dielectric space of the meta-material design [33]. The developed composites with RGO-SiC-LLDPE in different wt.% ratios are listed in Table 1.

2.3 Microstructural analysis

Microstructural studies of the developed RGO and as received SiC samples were carried out using X-ray diffraction (XRD) (Rigaku miniflex, Cu Kα, 1.54) and illustrated in Figure 1. A prominent peak at $2\theta = 10.35^{\circ}$ is observed for GO corresponding to (0 0 1) diffraction planes [34]. A diffraction peak at around $2\theta = 23.96^{\circ}$ is distinguishable for RGO which indicates the highly amorphous nature of RGO while the peak at $2\theta = 10.35^{\circ}$ has disappeared, which indicates the removal of oxygen-containing functional groups during the reduction of GO into RGO. The XRD pattern of as received SiC samples shows similar peaks as illustrated in reference [35].

To further confirm the synthesis of RGO, optical absorption spectra of suspended RGO were obtained as illustrated in Figure 1b. The spectrum of RGO showed characteristic peak at 269 nm which can be attributed to removal of oxygen functional groups and restoration of conjugated structure [36]. FESEM image of reduced graphene oxide shown in Figure 2a exhibits wrinkled like structure that caused sheet folding. Due to decomposition of oxygen-containing groups, carbon atoms from the carbon plane have been removed consequently splitting of graphene sheets into small pieces and distortion of the carbon plane occurs. The FESEM image, Figure 2b shows that the SiC particles are of varying shapes and sizes. The Figure 2c shows the FESEM image of RGO-SiC-LLDPE composite with limited agglomerated filler distribution within the LLDPE matrix.

2.4 Microwave characterization

The constitutive parameters of the dispersive material medium viz. complex permittivity, $\varepsilon_r(\omega)$ and permeability,

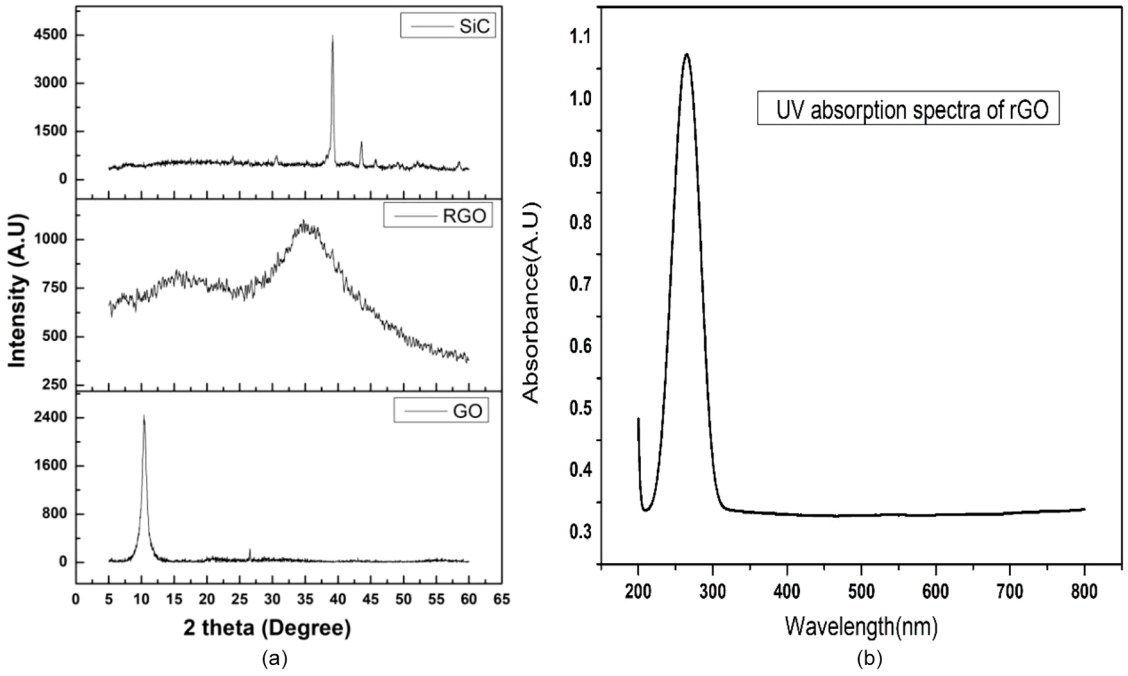

Fig. 1. (a) XRD patterns of GO, RGO, SiC and (b) UV–Vis spectrum of RGO.

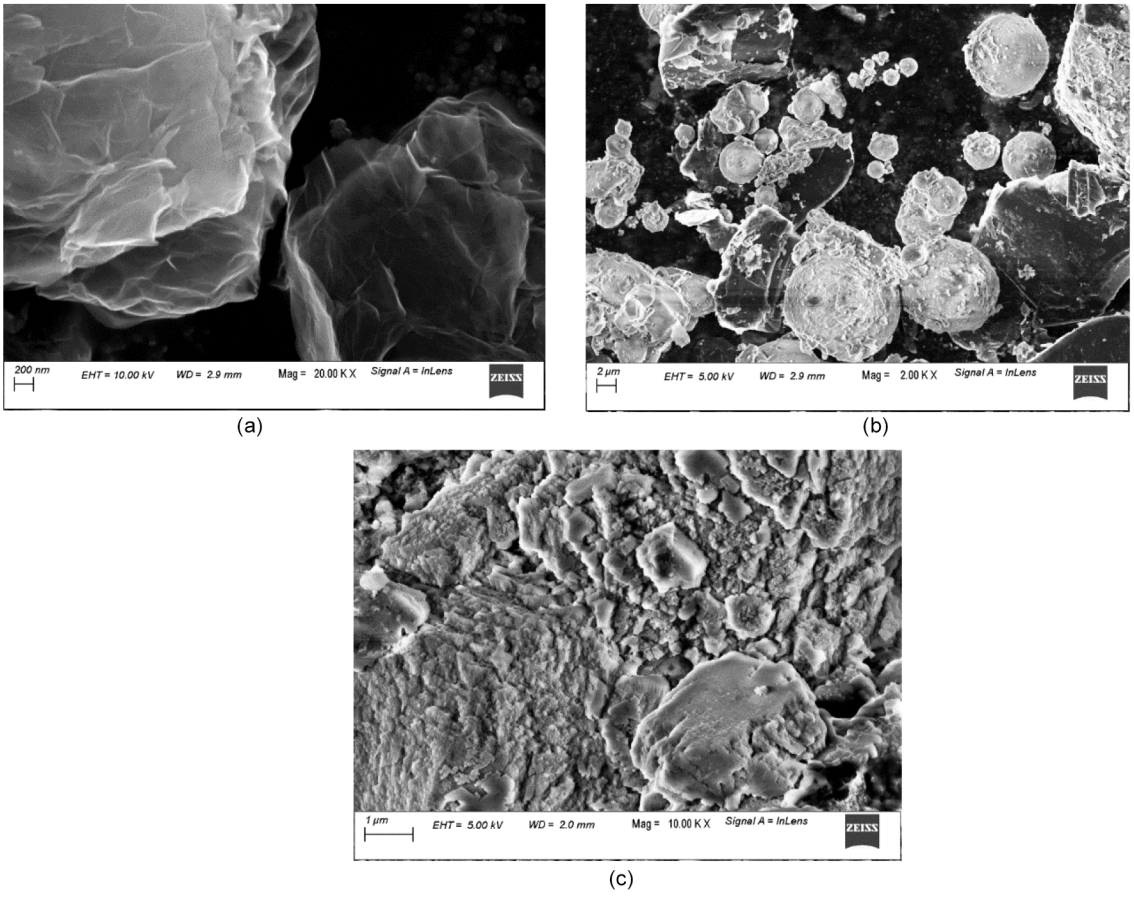

Fig. 2. SEM images of (a)RGO, (b) SiC, (c) RGO-SiC-LLDPE composite.

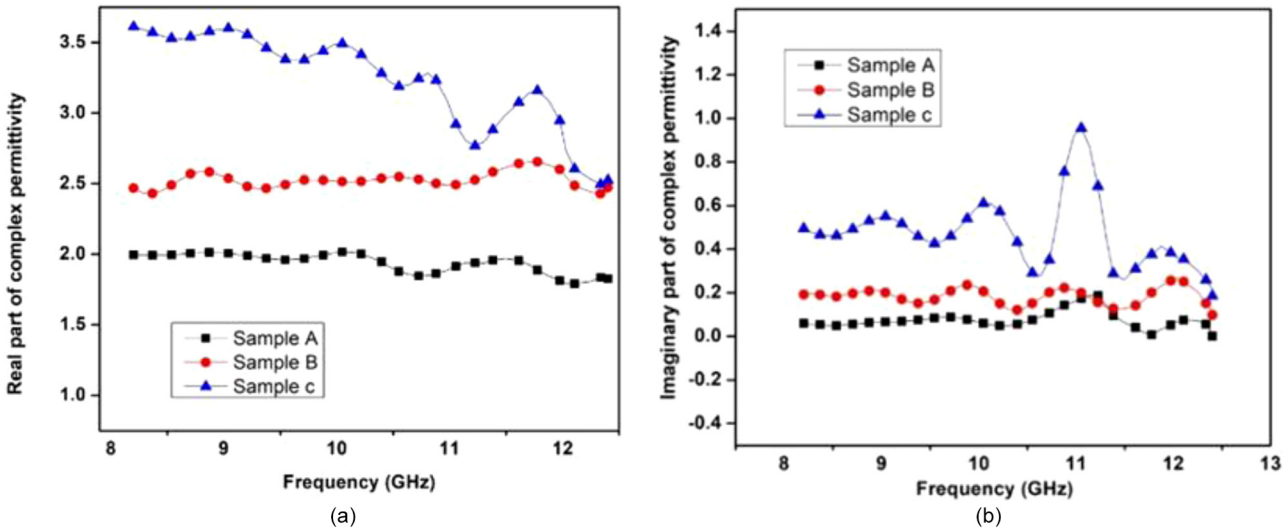

Fig. 3. Complex permittivity of RGO-SiC-LLDPE composite; (a) real permittivity and (b) imaginary permittivity.

$\mu_r(\omega)$ determine the propagation of the electromagnetic wave through the medium and in designing meta-material structure the substrate may take part a major role in microwave absorption. Measurement of $\varepsilon_r(\omega)$ and $\mu_r(\omega)$ values of the developed composites samples (A, B C) were carried out using Nicolson and Ross [37] method employing Agilent 85071E material measurement software compatible with Agilent E8362C VNA in the X-band, as shown in Figure 3. The composites are found to be non-magnetic as indicated by $(\mu_r(\omega) = 1 - \mathrm{j}.0)$. As observed from Figures 3a and 3b, $\varepsilon_r^{/}(\omega)$ and $\varepsilon_r^{//}(\omega)$ values enhance over the X-band with increase in filler concentrations (RGO-SiC) in the composite. The values of $\varepsilon_r^{/}(\omega)$ Figure 3a increase from 2.0 for the composite sample A (RGO-SiC, 10%) to 3.7 for the composites sample C (RGO-SiC, 20–10%) at 8.2 GHz. Figure 3a also indicates that the $\varepsilon_r^{/}(\omega)$ values for the composites sample A(RGO-SiC, 10%) and B (RGO-SiC, 20%) with lower concentration of fillers are almost frequency independent in the entire range of X-band. However, there is a declining trend in the values of real part of permittivity $\varepsilon_r^{/}(\omega)$ of the sample C with higher amount of filler (RGO-SiC, 20–10%) from 3.7 (8.2 GHz) to 2.5 at 12.4 GHz with frequency. Similar trend has been observed in Figure 3b for the values of imaginary part of permittivity $\varepsilon_r^{//}(\omega)$, the $\varepsilon_r^{//}(\omega)$ values for the composite samples A and B with lower concentration of fillers exhibit more or less frequency independent character in the frequency range 8.2–12.4 GHz. However with fillers concentration in the samples, $\varepsilon_r^{//}(\omega)$ values rise from 0.1 (sample A (RGO-SiC, 10%)) to 0.5 (sample C (RGO-SiC, 20–10%)) at 8.2 GHz. Similar to $\varepsilon_r^{/}(\omega)$ values, the $\varepsilon_r^{//}(\omega)$ values of sample C too exhibits frequency dispersive behavior with an unsteady declining trend with frequencies, the values fall from 0.5 at 8.2 GHz to 0.19 at 12.4 GHz along with resonance peak values 0.7 at 10 GHz and 1.0 at 11 GHz. Since permittivity of a dielectric medium is a measure of the polarizability, hence, samples with higher amount of (RGO-SiC) in the LLDPE matrix may enhance the conductivity and dielectric polarization which in turn promotes the complex permittivity values. The real part of the complex permittivity of the samples A–C related to energy absorbed can be mainly ascribed to the orientational and interfacial polarization and the presence of the bound charges and space charge polarization effect in heterogeneous composites (RGO-SiC) filler in the samples are expected to be responsible for enhancement of this part of the complex permittivity. Because of the high electron conductivity property of RGO [38], free electrons can travel freely within it and accumulate at the RGO-SiC interface, the heterogeneous RGO-SiC composite systems thus build up boundary-layer capacitors which generates the interfacial polarization [39]. The imaginary part $\varepsilon_r^{//}(\omega)$ of the complex permittivity responsible for the dissipation of EM energy in the form of heat (relaxation and ohmic loss) also increases with fillers concentration in the samples, which can be attributed to the improvement in electric conductivity of the samples with higher amount of rGO. Both the polarizations orientational and interfacial leads to the energy loss mechanism of irradiated radiation due to formation of huge dipoles with the associated relaxation phenomenon [40]. As the dipole density and their orientation determine the polarizability of the composite material which in turn depends on the fillers concentration, so increase in frequency of the applied field results dipole relaxation because the large number dipoles present in the sample C unable to match their reorienting frequency with that of applied electric field in order to resist the oscillating field and as a result, complex permittivity of sample C declines with increasing frequency as in Figures 3a and 3b. Also interfacial polarization provides good support at lower frequency [40], with increase in frequency of applied field the tendency for the interfacial polarization [41] is also expected to be decreased resulting in decrease in polarizability and hence permittivity and loss factor. Because of high conductivity and polarization at RGO-SiC interfaces make it possible for electron transfer process [38] through dipole–dipole interactions by allowing electron hopping and transferring between the fillers and matrix, which also assists for microwave absorption. The frequency response plot of permittivity of Figures 3a and 3b indicates

Table 2. Optimized MA parameters.

Unit cell parameters	Values (in mm)
Outer radius of the ring	3.0
Inner radius of the ring	2.5
Thickness of the ring	0.2
Length of the substrate	22.86
Breadth of the substrate	10.16
Length of each of the rectangular strip along X-axis	8.63
Breadth of each of the rectangular strip along X-axis	0.8
Thickness of each of the rectangular strip along X-axis	0.2
Length of each of the rectangular strip along Y-axis	2.2
Breadth of each of the rectangular strip along Y-axis	0.8
Thickness of each of the rectangular strip along Y-axis	0.20
Thickness of the substrate	Variable for different substrates

similar trend for both $\varepsilon_r^{/}(\omega)$ & $\varepsilon_r^{//}(\omega)$ values in the lower − frequency range with prominent resonance peaks for the sample C at 11.7 GHz for $\varepsilon_r^{/}(\omega)$ and at 10.1 & 11.1 GHz for $\varepsilon_r^{//}(\omega)$ towards higher − frequency range. High conductivity and significant skin effect of composites are responsible for resonance behavior [42]. High conductivity of sample C in the study related to resonance is owing to the presence of higher amount of RGO. In the lower-frequency range usually resonance behavior is expected from large number of defects such as vacancy or pores provided that space charges are present in the medium. In the higher-frequency range resonance behavior of complex permittivity is estimated from electronic and atomic polarizations [42]. Polarization and various intrinsic nature of composite material can thus be responsible for observed peaks in the plot of both the real $(\varepsilon_r^{/}(\omega)$ and imaginary $\varepsilon_r^{//}(\omega)$ parts of complex permittivity. Moreover, the frequency dependence composites complex permittivity behavior of various wt.% of RGO-SiC fillers can be analyzed through capacitor formalism of composites [41]. Polymer with inclusion of composite fillers may be regarded as a parallel network of large number of boundary layer parallel capacitors. Enhances in capacitance is attributed to enhance static permittivity of the material through higher wt.% fillers inclusion. However, in the presence of alternating field, capacitance being proportional to permittivity becomes a complex function exhibits frequency dependence character. Current through the capacitor is controlled by its reactance which reduces with frequency, that is, sample becomes frequency controlled resistor.

2.5 Design and simulation

X-band meta-material microwave absorber of ring shape with four stripe structure, shown in Figure 4 is designed on the developed RGO-SiC-LLDPE composites as well as on standard FR4 substrate using electromagnetic simulator, CST Microwave studio. Simulation is performed for transverse electric mode with normal incidence only and

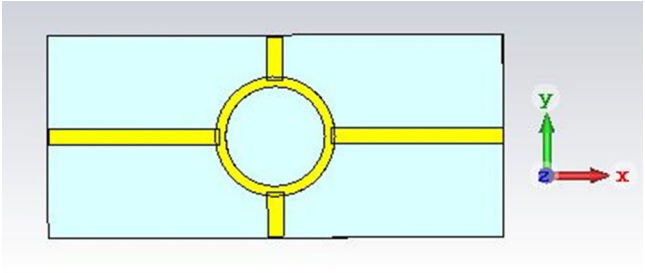

Fig. 4. Proposed MA structure.

considering the periodic boundary conditions applied along X- and Y- direction and the plane electromagnetic wave along Z-direction as shown, inset in Figure 4. The optimized parameters of the design with different substrate material are given in Table 2. The frequency dependent $S_{11}(\omega)$ values of the optimized design on different substrate viz. FR4, sample A, sample B and sample C with varied thickness (d) are plotted in Figures 5a–5d. It has been observed from Figure 5a, that the proposed design on FR4 substrate of $d = 0.5$ mm shows excellent $S_{11} \sim -90$ dB in the C-band and $S_{11} \sim -18$ dB at 8.3 GHz. However, the optimized design shows $S_{11} \sim -48$ dB at 10.98 GHz, $S_{11} \sim -22$ dB at 10.3 GHz, $S_{11} \sim -18$ dB at 8.7 GHz on sample A, sample B and sample C substrates. From the simulated results the role of dielectric substrate on S11 (ω) values are prominently observed as shifting of absorption peak takes place towards the X band frequency range. This shifting of resonance peak $\left(f = \frac{1}{2\pi\sqrt{LC}}\right)$ may be attributed to the change in capacitance of the composites samples. From Figure 3, the values of complex permittivity increases from sample A to sample C, which in turn increases the capacitance of the metamaterial structure and hence resonating frequency shifted towards lower frequency range from sample A to sample C. Moreover, the simulated surface current distribution at different resonance

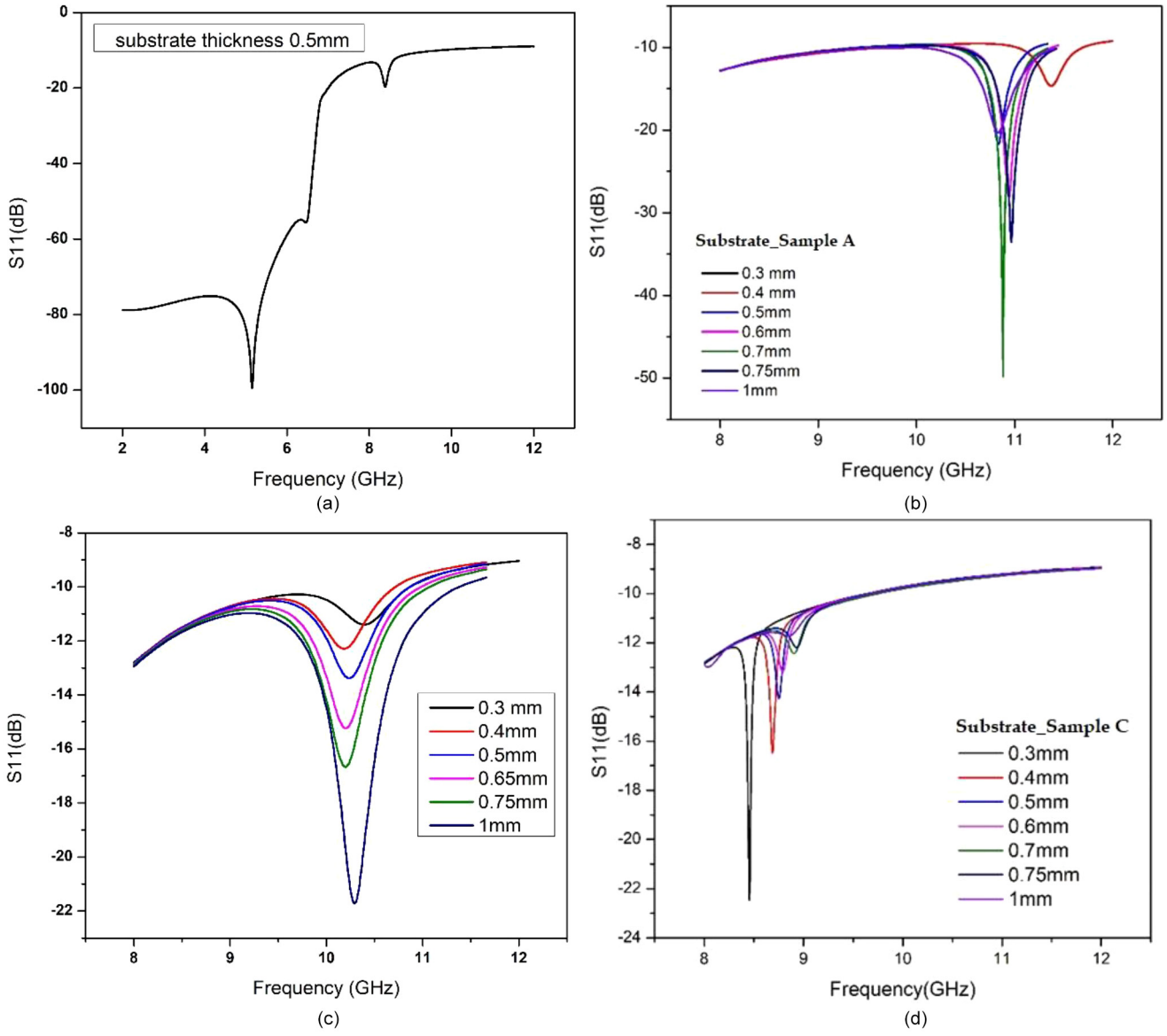

Fig. 5. Simulated S11 (ω) values of the proposed MA design on (a) FR4, (b) Sample A, (c) Sample B, (d) Sample C substrate.

frequencies on the front and back layers of the unit-cell structure have been simulated, as shown in Figures 6a–6d exhibits strong electric dipole on front layer corresponds to the external electric field of the incident EM wave, and the magnetic dipole response excited between the front and back layers of the unit-cell by the magnetic field of the incident EM wave. It has been observed that with increasing conductive filler concentration in the dielectric spacer, the surface current distribution become less prominent. Apart from material parameters, the magnitude of S11 (ω) values vary for different thicknesses of the developed substrate along with frequency shifting of the peak values. It may be attributed to guide wavelength within the dielectric spacer between the front and back layer of the metamaterial structure. Further, the absorption mechanism can be explained on basis of slow wave effect of the metasurface by the trapping the electromagnetic wave inside the structure for prolong interaction as reported by Li et al. [43]. The group refractive index of the metamaterial structures developed on sample A, sample B and sample C are calculated using electromagnetic simulator, CST Microwave studio and found to be 1.4, 1.45 and 2.5 respectively.

2.6 Fabrication and experimental verification of the proposed MA design

The proposed design is fabricated on the developed substrate and on standard FR4 substrate using Cu-substrate (99%, Klim) of 0.2 mm thickness as shown in Figure 6a. Initially composites of RGO-SiC-LLDPE composites of variable thickness were prepared and optimized MA structure of dimension 15 cm × 15 cm with conductor backed ground plane was fabricated. The free

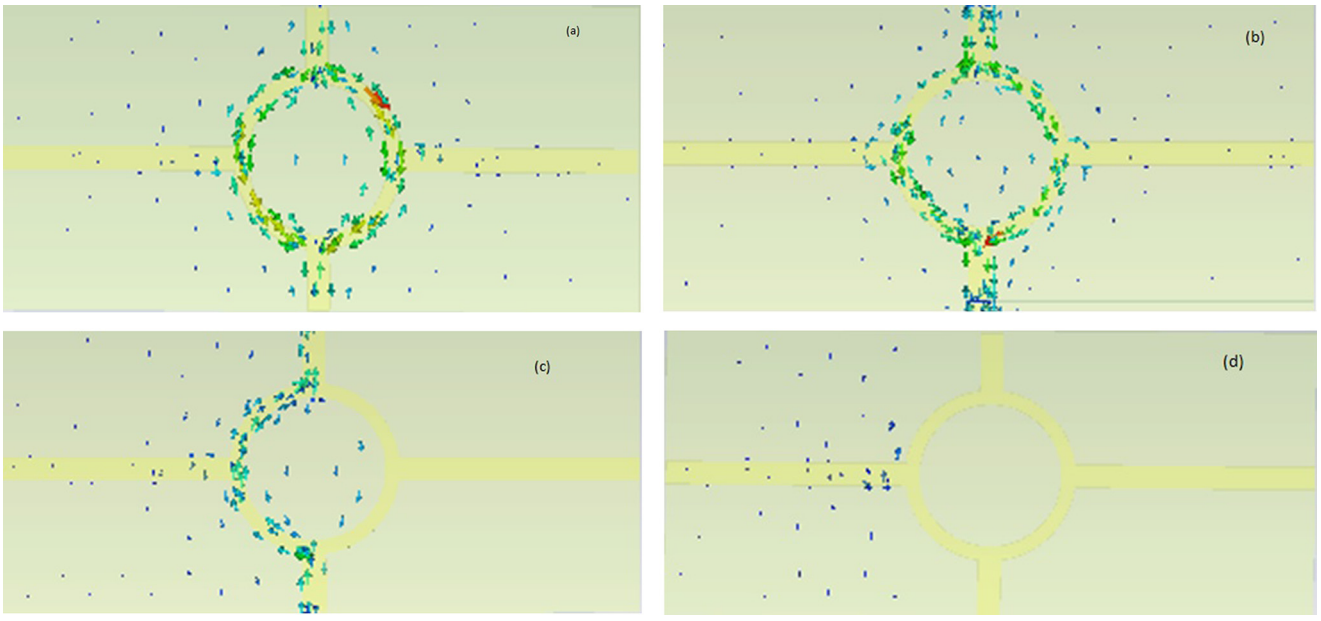

Fig. 6. The simulated surface current distributions of the unit-cell structure of the proposed metamaterial at different resonance frequencies: (a) FR4 at 7 GHz, (b) Sample A at 9.6 GHz, (c) Sample B at 8.31 GHz, (d) Sample C at 8.34 GHz.

space microwave absorption testing was performed using Agilent E8362C Vector Network Analyzer calibrated through TRL technique [44].The experimental S11 (ω) curves plotted in Figure 6b showed S11∼−25, −22 and −16 dB at 10.7 GHz with −10 dB absorption bandwidth of ∼0.29, 0.31 and 0.16 GHz for MA design with sample A, sample B and sample C substrate, however, no prominent peak was obtained for the design with FR4 substrate. The simulated and experimental results were differ in resonant frequency since in simulation, periodic boundary condition assumes was infinite however in real, finite dimension cause edge diffraction which result in shifting of resonant frequency [45]. For the proposed metamaterial design, the resonant frequency is given as $f = \frac{1}{2\pi\sqrt{LC}}$ where L and C represent inductance and capacitance of the meta-material structure respectively. Moreover, it has been observed that with increase wt.% of the substrate the S11 value decrease for the design which may be attributed lossy characteristic of the substrate which disturb the impedance matching condition of the electromagnetic wave propagating through the substrate. Figure 7c shows the maximum absorption of 96.7% at 10.7 GHz for the substrate A. Practically it has been observed that the transmission of irradiated radiation take place through impedance matching conditions at the air MMA surfaces at 10.7 GHz for all the dielectric substrates (A–C). Moreover, for the MMA having composite substrate A indicates enhance absorption of incident radiation compared to other two samples, it is because, the thickness of substrates plays the role of absorption through quarter wave $\left(\frac{\lambda_g}{4}\right)$ phase cancellation, $\lambda_g = \frac{\lambda_0}{\sqrt{\varepsilon_r}}$ being guided wave length in the medium. Sample A with greater thickness 0.7 mm provides more odd multiple wavelength path $d = (2n+1)\ \frac{\lambda_g}{4}$ [46] for the transmitted and reflected attenuated waves from the surface backed by conductor for phase cancellation and their by promotes absorption compared to the other two samples of 0.5 and 0.7 mm thickness. Further, guided wave length $\lambda_g = \frac{\lambda_0}{\sqrt{\varepsilon_r}}$ with λ_0 and $\sqrt{\varepsilon_r}$ values at 10.7 GHz determined from the Figure 3, provides almost equal wavelength for all the composite substrates which may be responsible for occurring of absorption peaks at the almost same resonance absorption frequency of 10.7 GHz.

3 Conclusion

The present work developed a novel material based on RGO-SiC-LLDPE composites for viable application as substrate in designing meta-material microwave absorber. A novel meta-material design of ring shape with four stripe structure is designed and simulated on the developed as well as standard FR4 substrate. The results shows S11∼−25, −22 and −16 dB at 10.7 GHz are observed for composites samples A, B and C respectively with maximum absorption of 96.7% at 10.7 GHz for the substrate A. The role of substrate parameters with thickness consideration influences the resonant peak of the meta-material design. Considering the overall performance of the MA design with limited thickness <1 mm could be a potential microwave absorber for X-band frequency range.

The authors would like to sincerely thank Microwave Engineering Laboratory, Department of Physics, Tezpur University, Assam for providing the possible laboratory facilities and CST studio simulation software.

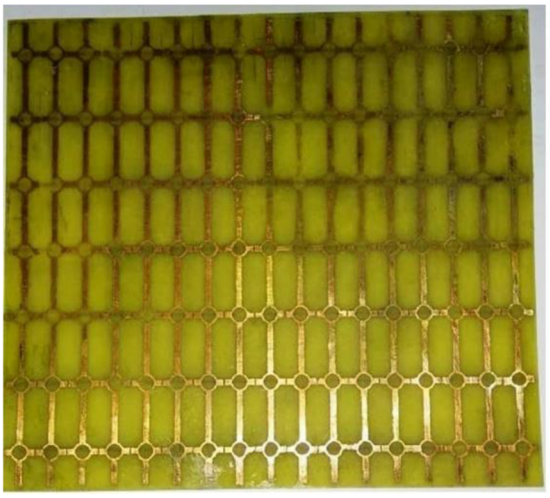

(a)

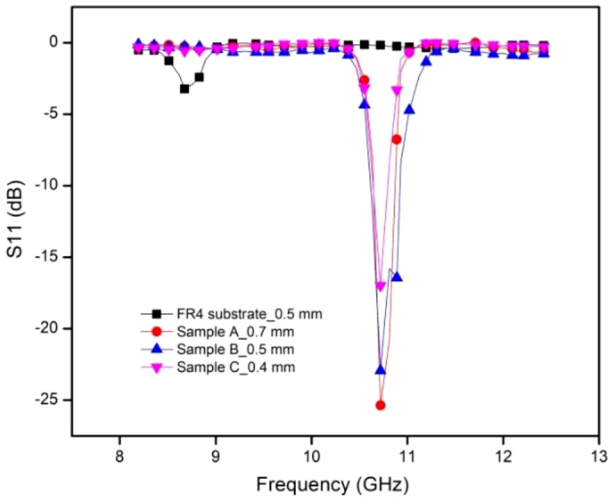

(b)

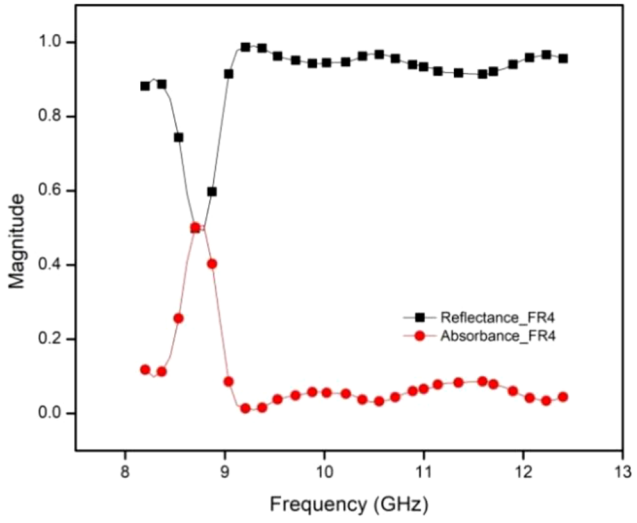

(c)

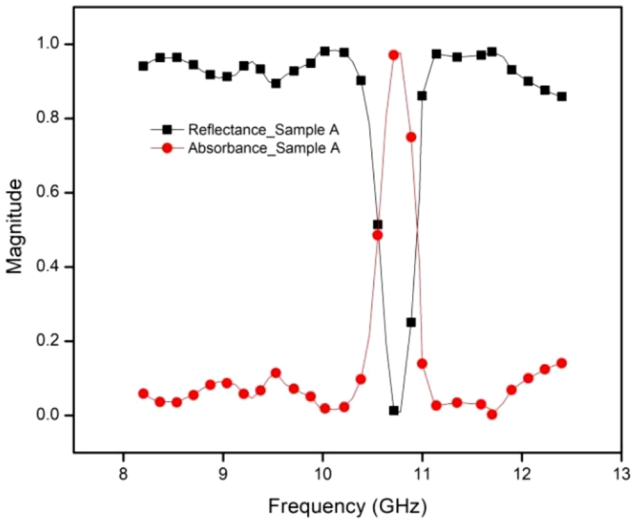

(d)

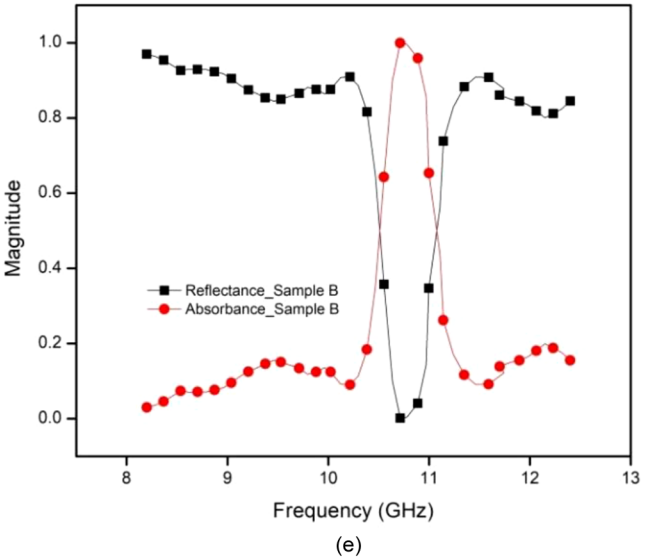

(e)

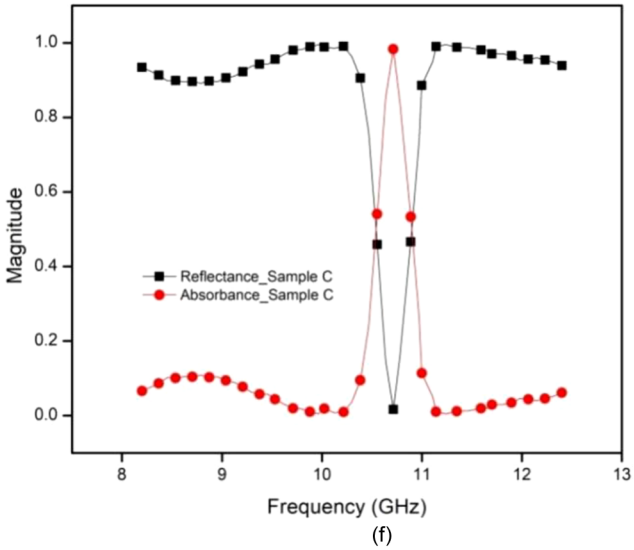

(f)

Fig. 7. (a) Fabricated sample, (b) measured S11 (ω) values, (c–f) reflectance and absorbance of the proposed MA.

References

1. X.C. Tong, Advanced materials and design for electromagnetic interference shielding (CRC Press, Taylor and Francis, New York, 2009)
2. F. Qin, C. Brosseau, J. Appl. Phys. **111**, 061301 (2012)
3. C.M. Watts, X. Liu, W.J. Padilla, Adv. Mater. **24**, OP98 (2012)
4. P.K. Singh, K.A. Korolev, M.N. Afsar, S. Sonkusale, Appl. Phys. Lett. **99**, 261101m (2011)
5. N.I. Landy, S. Sajuyigbe, J.J. Mock, D.R. Smith, W.J. Padilla, Phys. Rev. Lett. **100**, 207402 (2008)
6. B. Zhu, C. Huang, Y. Feng, J. Zhao, T. Jiang, Prog. Electromagn. Res. B **24**, 121 (2010)
7. C.M. Bingham, H. Tao, X. Liu, R.D. Averitt, X. Zhang, W.J. Padilla, Opt. Express **16**, 18565 (2008)
8. G.T. Ruck, D.E. Barrick, W.D. Stuart, Radar Cross Section Handbook (Plenum, New York, 1970)
9. J.W. Park, P.V. Tuong, J.Y. Rhee, K.W. Kim, W.H. Jang, E.H. Choi, L.Y. Chen, Y.P. Lee, Opt. Express **21**, 9691 (2013)
10. Y.J. Yoo, Y.J. Kim, P.V. Tuong, J.Y. Rhee, K.W. Kim, W.H. Jang, Y.H. Kim, H. Cheong, Y.P. Lee, Opt. Express **21**, 32484 (2013)
11. F. Ding, Y. Cui, X. Ge, Y. Jin, S. He, Appl. Phys. Lett. **100**, 103506 (2012)
12. Y.J. Kim, Y.J. Yoo, K.W. Kim, J.Y. Rhee, Y.H. Kim, Y.P. Lee, Opt. Express **23**, 3861 (2015)
13. Y.J. Kim et al., J. Phys. D Appl. Phys. **49**, 435102 (2016)
14. R. Pelluri, B. Appasani, Prog. Electromagn. Res. Lett. **69**, 59 (2017)
15. T.H. Nguyen et al., Adv. Nat. Sci. Nanosci. Nanotechnol. **5**, 025013 (2014)
16. R. Yahiaoui, H.H. Ouslimani, J. Appl. Phys. **122**, 093104 (2017)
17. T.S. Tuan, N.T.Q. Hoa, AIP Adv. **9**, 055321 (2019)
18. S. Bhattacharyya, S. Ghosh, K.V. Srivastava, J. Appl. Phys. **114**, 094514 (2013)
19. W. Wang, M. Yan, Y. Pang, J. Wang, H. Ma, S. Qua, H. Chen, C. Xu, M. Feng, Appl. Phys. A **118**, 443 (2015)
20. W.G. Dong, L.M. Hai, H.X. Wei, K.L. Hua, C.L. Li, C.Z. Quan, Chin. Phys. B **23**, 017802 (2013)
21. L. Li, Y. Yang, C. Liang, J. Appl. Phys. **110**, 063702 (2011)
22. O. Ayop, M.K.A. Rahim, N.A. Murad, H.A. Majid, Appl. Phys. A **117**, 651 (2014)
23. R. Pelluri, B. Appasani, Prog. Electromagn. Res. Lett. **69**, 59 (2017)
24. B.S. Tung, B.X. Khuyen, Y.J. Kim, V.D. Lam, K.W. Kim, Y.P. Lee, Sci. Rep. **7**, 11507 (2017)
25. G. Sen, M. Kumar, S.k.N. Islam, S. Das, Wave Random Complex Media **29**, 153 (2019)
26. D. Sood, C.C. Tripathi, J. Microwave, Optoelectron. Electromagn. Appl. **16**, 514 (2017)
27. K. Kumari, N. Mishra, R.K. Chaudhary, Microw. Opt. Technol. Lett. **59**, 2664 (2017)
28. D. Borah, N.S. Bhattacharyya, J. Electron. Mater. **46**, 226 (2017)
29. C. Wang, X. Han, P. Xu, X. Zhang, Y. Du, Appl. Phys. Lett. **98**, 072906 (2011)
30. H.J. Yang, J. Yuan, Y. Li, Z.L. Hou, H.B. Jin, X.Y. Fang, M.S. Cao, Solid State Commun. **163**, 1 (2013)
31. W.S. Hummers, R.E. Offeman, J. Am. Chem. Soc. **80**, 1339 (1958)
32. N. Cao, Y. Zhang, J. Nanomater. **2015**, 168125 (2015)
33. P.J. Gogoi, S. Bhattacharyya, N.S. Bhattacharyya, J. Electron. Mater. **44**, 1071 (2015)
34. D.Y. Pan, S. Wang, B. Zhao, M.H. Wu, H.J. Zhang, Y. Wang, Z. Jiao, Chem. Mater. **21**, 3136 (2009)
35. A.L. Ortiz, F. Sanchez-Bajo, F.L. Cumbrera, F. Guiberteau, Mater. Lett. **49**, 137 (2001)
36. S. Sunderrajan, L.R. Miranda, G. Pennathur, Prep. Biochem. Biotechnol. **48**, 343 (2018)
37. A.M. Nicolson, G. Ross, IEEE Trans. Instrum. Meas. **19**, 377 (1970)
38. Y. Zhang, S. Gao, H. Xing, J. Alloy. Compd. **777**, 544 (2019)
39. X.F. Zhang, P.F. Guan, X.L. Dong, Appl. Phys. Lett. **96**, 223111 (2010)
40. U.J Mahanta, J.P Gogoi, D. Borah, N.S. Bhattacharyya, IEEE Trans. Dielectr. Electr. Insul. **26**, 194 (2019)
41. U.J. Mahanta, N.S. Bhattacharyya, I. Hussain, P.J. Gogoi, J.P. Gogoi, J. Phys. Chem. Solids **127**, 202 (2019)
42. Y. Li, R. Wang, F. Qi, C. Wang, Appl. Surf. Sci. **254**, 4708 (2008)
43. Z. Li, B. Li, Q. Zhao, J. Zhou, AIP Adv. **10**, 045311 (2020)
44. G.F. Engen, C.A. Hoer, IEEE. Trans. Microw. Theory Tech. **27**, 987 (1979)
45. X. Huang, H. Yang, S. Yu, J. Wang, M. Li, Q. Ye, J. Appl. Phys. **113**, 213516 (2013)
46. L. Zhang, H. Zhu, Y. Song, Y. Zhang, Y. Huang, Mater. Sci. Eng. B **153**, 78 (2008)

Cite this article as: Pankaj Bora, Utpal Jyoti Mahanta, Jayanta Kumar Sarmah, Jyoti Prasad Gogoi, X-band metamaterial absorbers based on reduced graphene oxide-silicon carbide-linear low density polyethylene composite, EPJ Appl. Metamat. **7**, 8 (2020)